Comparative Study on Transparency Retrieved From GOCI Under Four Different Atmospheric Correction Algorithms in Jiaozhou Bay and Qingdao Coastal Area

Xiao-Yan Liu, Jing-Wen Hu, Lin Tian, Ding-Feng Yu, Hao Gao, Lei Yang, and De-Yu An

***Abstract*—Water transparency is one of the important parameters to describe the optical properties of seawater. It is a visual reflection of the degree of turbidity of seawater and the degree of absorption and scattering of light by seawater. First, this article verified and analyzed the suitability of the water transparency retrieval method proposed by Lee in 2015 (denoted as Zsd_lee_2015) for Jiaozhou Bay and Qingdao offshore waters by using the in-situ data. Second, the water transparency estimation results retrieved from Geostationary Ocean Color Imager (GOCI) using four atmospheric correction (AC) algorithms were compared and analyzed with in-situ data in the study area. The four AC algorithms are the standard AC algorithms of Korea Ocean Satellite Center (KOSC) GOCI GDPS1.3 and GDPS2.0, the standard near-infrared AC algorithm of NASA, and management unit of the North Sea mathematical models. At last, GOCI data on Mar 09, 2018, were used to analyze the differences in hourly changes of transparency caused by different AC algorithms in detail. The results show that the Zsd_lee_2015 model is suitable for the study area (R^2>0.8, MAPE = 16.4%). The difference in transparency value caused by the AC algorithm cannot be ignored completely. Moreover, there are great differences in the moment when the maximum value of transparency is presented based on different AC algorithms, while the moment when the minimum value of transparency is presented is basically the same, mostly occurring at 00:16. The results cast doubt on the previous conclusions about the hourly variations of biochemical parameters using GOCI because the hourly variations obtained under different AC algorithms are not completely consistent.**

***Index Terms*—Atmospheric correction (AC), geostationary ocean color imager (GOCI), hourly change, Jiaozhou bay and Qingdao coastal area, water transparency.**

Manuscript received 1 June 2023; revised 21 September 2023; accepted 30 November 2023. Date of publication 15 December 2023; date of current version 29 December 2023. This work was supported in part by the National Key Research and Development Program of China under Grant 2020YFE0201900, in part by the National Natural Science Foundation of China under Grant 42106172, in part by the Special Foundation for Young Scientists of National Satellite Meteorological Center, China Meteorological Administration under Grant 202204QT084, in part by the Natural Science Foundation of Shandong Province under Grant ZR2021QD135, Grant ZR2019PD021, Grant ZR2023QD066, Grant ZR2022QD061, and Grant ZR2023QD023, and in part by the Project Plan of Pilot Project of Integration of Science, Education and Industry of Qilu University of Technology (Shandong Academy of Sciences) under Grant 2022GH004, Grant 2022PY041, Grant 2023PX035, Grant 2023PX094, Grant 2023RCKY051, and Grant 2023RCKY047. *(Corresponding author: Lin Tian.)*

Xiao-Yan Liu is with the Institute of Oceanographic Instrumentation, Qilu University of Technology (Shandong Academy of Sciences), Qingdao 266000, China, and with the College of Information Science and Engineering, Ocean University of China, Qingdao 266100, China (e-mail: liuxiaoyan@qlu.edu.cn).

Jing-Wen Hu is with the Shandong Marine Forecast and Hazard Mitigation Service, Qingdao 266590, China (e-mail: hujingwen@shandong.cn).

Lin Tian is with the National Satellite Meteorological Center, China Meteorological Administration, Beijing 100000, China (e-mail: tianl@cma.gov.cn).

Ding-Feng Yu, Hao Gao, Lei Yang, and De-Yu An are with the Institute of Oceanographic Instrumentation, Qilu University of Technology (Shandong Academy of Sciences), Qingdao 266000, China (e-mail: dfyu@qlu.edu.cn; gaohao88_sdioi@qlu.edu.cn; yangleibest@qlu.edu.cn; dyan@qlu.edu.cn).

Digital Object Identifier 10.1109/JSTARS.2023.3343572

I. Introduction

WATER transparency, also known as Secchi Disk depth (Zsd, m), is one of the important parameters describing the optical properties of seawater. With the development of marine technology, the application of seawater transparency has become more widespread and has wide implications from water quality to climate change research [1], [2], [3], [4], [5]. First, the change characteristics of the water transparency can assist the studies of water mass analysis and sea water movement, as well as determining the range and number of fish activities [3]. Second, the transparency of seawater is a good indicator to identify the changes in marine water quality. It is one of the parameters that must be measured in the monitoring of red tide, oil spill, and monitoring of the environmental impact assessment of the construction port. Furthermore, the transparency of the seawater can also be used to retrieve the visible light's attenuation coefficient and the diffuse attenuation coefficient to obtain the euphotic depth of the seawater to estimate the primary productivity of the water body [2], [4]. Therefore, to monitor the temporal and spatial variation of seawater transparency is of great significance for studying the physical and chemical properties of seawater, fishery production, marine ecological monitoring, and naval military activities [6], [7].

The traditional seawater transparency monitoring is based on manual in-site observation, measured with a white or black-and-white disc of 30 cm diameter to obtain the depth at which a Secchi disc falls vertically into the water and just disappears from the human eye [10]. Based on this method, only the localized water transparency can be understood. The demands for large-scale, rapid, and real-time monitoring of ocean elements cannot be met. Satellite remote sensing technology has the characteristics of rapid and periodic, which can acquire a wide range of seawater

transparency distribution characteristics efficiently on time, and make up for the defects of traditional monitoring methods of seawater transparency [8]. At present, many scholars have used satellite remote sensing data to retrieve the transparency of seawater, and proposed various methods of seawater transparency monitoring based on remote sensing inversion. Prasad et al. [9] found a good correlation between seawater transparency and the ratio of the two-band water-leaving radiances by analyzing a large amount of water color data. Kratzer et al. [10] proposed the calculation of seawater transparency by the diffuse attenuation coefficient in the vertical direction and applied the method to the transparency measurement of the Baltic Sea. Doron et al. [11] proposed a method for measuring vertical visibility using remote sensing methods. And this method establishes a method for calculating the optical parameters of seawater transparency by inherent optical properties obtained by remote sensing inversion. Lee et al. [12], [13] proposed a new theoretical model (Zsd_lee_2015) for water transparency inversion in 2015 and applied 338 globally measured remote sensing reflectance (R_{rs}) and secchi disk depth (Zsd) field-measured data sets for verification analysis and extended application to Landsat-8 satellite remote sensing observation data. Shang et al. [14] applied Lee_2015's water transparency retrieve algorithm to MODIS (MODerate resolution Imaging Spectroradiometer) satellite observation data to analyze the water transparency of long-term sequences in the Bohai Sea. Lee et al. [15] used the new Zsd retrieval model to the relationship between Zsd and Chla (Chlorophyll-a). Jiang et al. [16] proposed an algorithm to retrieve Zsd from R_{rs} in various waters based on the new underwater visibility theory. Keivan Kabiri [17] proposed a method for the estimation of Zsd based on MODIS Kd(490) data and apply it in the northern Persian Gulf, the Strait of Hormuz, and the Gulf of Oman. Many other researchers have studied the spatial and temporal distributions of transparency in global oceans, and inland waters [18], [19], [20], [21], [22], [23], [24], [25], [26], [27], [28]. However, few scholars discuss the influence of different atmospheric correction (AC) algorithms on the accuracy of retrieved transparency. The ratio of water-leaving radiance to downwelling irradiance above the sea surface is defined as R_{rs}, which cannot be measured directly. However, the high precision of marine bio-optical parameters retrieved from satellite remote sensing data requires accurate R_{rs} data as the inputs (such as transparency retrieve research) [29]. For ocean color remote sensing, the water-leaving radiance of seawater contributes less than 10% of the total signal received by satellite ocean color sensor, while about 90% of the total signal received by the sensor is contributed from the atmosphere [30], [31], [32]. Therefore, we need to do AC for the received signal to remove the atmospheric signals and obtain water-leaving radiance or R_{rs} (λ), which is one of the key technologies of ocean color remote sensing. Accurate AC is the prerequisite for obtaining high-precision R_{rs} data and getting high-precision water color products [30]. At present, the AC algorithms for the case II water bodies include bright and dark pixel methods [31], [33], [34], [35], [36], [37], [38], [39], [40], [41], [42], neural network methods [43], [44], [45], spectral matching methods and optimization methods [46], [47], [48], [49], etc. The error analysis of ocean color products obtained by applying different AC algorithms to the same sensor should also be one of the research contents that need to be paid attention to in ocean optical remote sensing.

TABLE I
MEASURING INSTRUMENTS AND PARAMETERS DURING JIAOZHOU BAY AND QINGDAO COASTAL AREA (BULE STATIONS IN FIG. 1)

Instruments	Parameters	Number
Hyperspectral radiometer	Upward radiance profile, Downward radiance profile	16
Hyperspectral absorption-attenuation meter	Absorption coefficient (a) profile, Attenuation coefficient (c) profile	16
Backscatter instrument	Backscatter coefficient (b_b) profile	16
Secchi Disc	Transparency	16

Over the past two decades or more, many countries around the world have launched a variety of space-based ocean color sensors for daily global ocean observations, such as sea-viewing wide field sensor (SeaWiFS), MODIS, medium-resolution imaging spectrometer, visible infrared imager radiometer sensor, and ocean and land color instrument. There is also the historic geostationary ocean color imager (GOCI). GOCI is the main sensor mounted on communication ocean and meteorological satellite (COMS). The high-frequency observations of GOCI make it possible to analyze the hourly changes of marine geochemical parameters compared with the traditional polar orbit ocean color satellite. It is helpful to monitor the hourly changes in water quality, red tide, and green tide in offshore waters [50], [51], [52]. Jiaozhou Bay is a semi-closed shallow water bay located in Shandong Peninsula with an area of nearly 500 square kilometers. It belongs to the western part of the Yellow Sea and is an important representative of the gulf ecosystem in the North Temperate zone. The bay is high in nutrients and is an excellent sea area for the growth and reproduction of fish, shrimp, and shellfish. It belongs to the planning scope of Marine pasture breeding area in Shandong Province, and its water optical properties are complex. The transparency semi-analytical retrieval model of Zsd_lee_2015 solves the problem of human eye observation of Secchi disk with optical theory. This model has obtained good performance after being validated with 338 concurrent global measurements of both R_{rs} and Zsd covering oceanic waters, including nearly 200 match-ups of R_{rs} and Zsd from the China seas [12]. However, whether this Zds_lee_2015 model can be directly applied to GOCI satellite data to retrieve transparency in the Jiaozhou Bay and Qingdao coastal area, and whether the difference in retrieval results caused by different AC model can be ignored during the whole retrieval process? In this study, based on this hypothesis and GOCI data in Jiaozhou Bay and Qingdao coastal area, the error analysis of the retrieve accuracy of transparency under different AC algorithms and the difference analysis of the hourly change results of transparency under different AC algorithms were analyzed.

II. DATA

A. *In-situ Data*

A two-day marine optical field experiment was conducted in Jiaozhou Bay and Qingdao offshore on Aug 13–14, 2014.

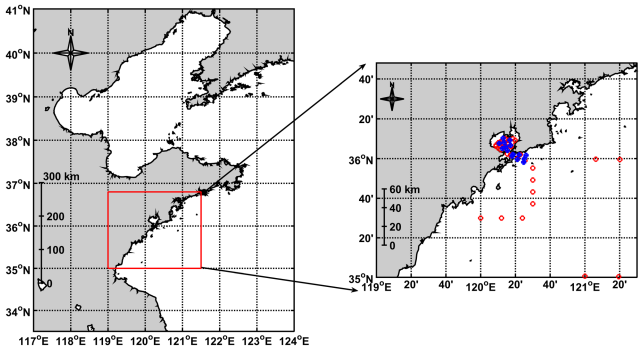

Fig. 1. Location map of in-situ stations in Jiaozhou Bay and Qingdao coastal area. The blue circles represent in-situ stations on Aug 13–14, 2014; the red circles represent stations of the measured transparency data provided by the Jiaozhou Bay Marine Ecosystem National Field Scientific Observation and Research Station in Shandong.

TABLE II
DATE OF MEASURED TRANSPARENCY IN JIAOZHOU BAY AND QINGDAO COASTAL AREA (RED STATIONS IN FIG. 1)

Date	Date
2013.08.19	2018.06.13
2014.04.28	2018.06.20
2015.09.10	2018.09.12
2017.05.16	2018.12.12
2018.03.12	2018.12.13
2018.03.09	

The stations are shown in blue circles (see Fig. 1). Experimental instruments and measurement parameters are listed (see Table I). Almost in each station, the parameters of the apparent optical parameters, for example, the upward radiance and the downward irradiance were measured, and then the R_{rs} data and the diffuse attenuation coefficient K_d data were derived. The intrinsic optical parameters were also measured: the absorption coefficient, the attenuation coefficient, and the backward scattering coefficient. And the transparency of seawater was measured too. The red dots in Fig. 1 are the stations of the measured transparency data provided by the Jiaozhou Bay Marine Ecosystem National Field Scientific Observation and Research Station in Shandong[1]

The local data time is shown in Table II.

B. GOCI/COMS Data

GOCI is the main sensor on South Korea's COMS satellite, which was launched in July 2010. It is the world's first geostationary ocean color satellite and covers China's Bohai Sea, Yellow Sea, and parts of the East China Sea and would captures 8 images per day from 8 A.M. to 3 P.M. in local time, one image per hour. The spatial resolution of GOCI observation is 500 m, and the spectral band ranges 412–865 nm (412, 443, 490, 555, 660, 680, 745, and 865 nm). Compared with the traditional polar orbit ocean color satellite, COMS/GOCI makes it possible to observe the diurnal variation of biogeochemical parameters, which is helpful to monitor the hourly variation of water quality, red tide, and green tide in offshore water. The GOCI L1B data were employed to estimate water transparency in this article, and the observation data are consistent with the field experimental data.

[1][Online]. Available: http://jzb.cern.ac.cn/

C. MODIS Data

MODIS is a key instrument aboard two NASA earth observing system satellites: Terra and Aqua. It has 36 spectral ranging from 140 to 1440 nm. In this article, MODIS/Aqua L1B data at the imaging time 05:25, Mar 09, 2018 (UTC) was used to get aot_555 data, which stands for Aerosol Optical Thickness at 555 nm, is an index parameter to characterize the amount of aerosol particles present in the atmosphere of the earth. The 555 nm wavelength range is chosen because it is sensitive to the scattering properties of most atmospheric aerosols.

III. ALGORITHM

A. AC Algorithms of KOSC GDPS

GDPS is the official software for processing GOCI data. The official website of KOSC currently provides global users with six versions (GDPS1.1, GDPS1.2, GDPS1.3, GDPS1.4, GDPS1.4.1, and GDPS2.0) of the installation program for free. The operational algorithm of AC for GDPS to process GOCI data adopts the bright pixel method, which is implemented by improving the iterative model for calculating near-infrared (NIR) water-leaving reflectance based on the standard SeaWiFS algorithm. Because of the absence of a short-wave infrared band in GOCI, GDPS1.1 and GDPS1.2 establish an empirical relation between the red band and the NIR water-leaving reflectance to calculate the NIR reflectance ρ_w [53], [54]. GDPS1.3 modifies the algorithm of GDPS1.1 and GDPS1.2, and increases the calculation order of the empirical relation of the water-leaving reflectance [55]. GDPS 1.4 mainly updates the modularization of the software based on GDPS 1.3. The AC of GDPS2.0 is different from the previous algorithms, which use the Spectral relationships in the aerosol multiple-scattering reflectance (SRAMS) spectral relations of aerosol multiple-scattering reflectance among different wavelengths to directly calculate the contribution of NIR multiple-scattering reflectance. Then the reflectance contribution of the NIR band to the visible band of the aerosol model was estimated by SRAMS spectrum [42].

In this article, the default AC algorithms of GDPS1.3 and GDPS2.0 are chosen to do AC on GOCI L1B data to obtain the $R_{rs}(\lambda)$ data to estimate transparency.

B. AC Algorithms of SeaDAS

NASA Ocean Biology Processing Group currently provides SeaDAS software for free to process oceanic remote sensing satellite data. SeaDAS provides multiple AC algorithms for users. The default AC algorithm of SeaDAS 8.2 (i.e., NASA standard AC algorithm, denoted as Seadas-Default) and management unit of the North Sea mathematical model (MUMM) AC algorithm (denoted as Seadas-MUMM) are used to conduct AC on GOCI L1B data in this article. Then the $R_{rs}(\lambda)$ data are obtained to estimate transparency. The NASA standard AC algorithm was originally developed by Gordon and Wang [56] in 1994, and was extended its application to case-2 waters by

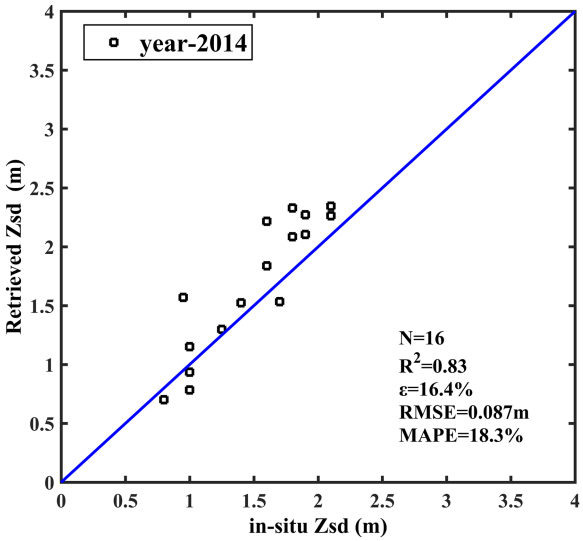

Fig. 2. Verification figure between the retrieved transparency values based on Zsd_Lee 2015 model using in-situ R_{rs} and K_d data and the in-situ measurement transparency data (blue stations in Fig. 1) in Aug 2014.

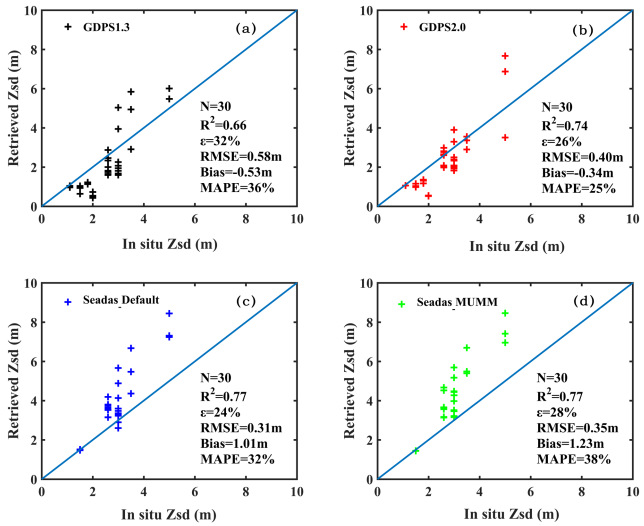

Fig. 3. Scatter plots between retrieved transparency data based on four different AC algorithms and measured transparency data (red stations in Fig. 1). (a) AC algorithm of GDPS1.3. (b) AC algorithm of GDPS2.0. (c) Standard AC algorithm of NASA. (d) AC algorithm of MUMM.

Stumpf et al in 2003 [57], and further was revised by Bailey and Ahmad et al in 2010 [58], [59]. NASA uses this algorithm as the default AC algorithm of SeaDAS to process the ocean color remote sensing data and provides L2 products for users. The MUMM AC algorithm was proposed by Ruddick in 2000 [31].

C. Water Transparency Retrieve Method

Lee et al. [12] proposed a new theoretical model of water transparency retrieval in 2015, and the derivation and verification are given in detail. It has been applied to MODIS and Landsat satellite data to retrieve seawater transparency successfully [13], [14]. The model formula is as follows:

$$Z_{\mathrm{sd}} = \frac{1}{2.5\mathrm{Min}(K_d(443, 488, 532, 555, 665))} \ln \times \left(\frac{|0.14 - R_{\mathrm{rs}}^{\mathrm{tr}}|}{C_t^r} \right). \quad (1)$$

Here $C_t^r = 0.013\ \mathrm{sr}^{-1}$ and it is the contrast threshold of a human eye for Secchi disk observation. $R_{\mathrm{rs}}^{\mathrm{tr}}$ is the remote-sensing reflectance (sr^{-1}) at the transparent window of the water body (the wavelength corresponding to the maximum transparency). K_d data were estimated from a and b_b data that can be obtained by Quasi-Analytical Algorithm Version 6.0 (QAA_V6) from R_{rs} [60].

This model was built and validated with 338 concurrent global measurements of both R_{rs} and Zsd, resulting in an averaged unbiased percentage difference $\varepsilon = 18.2\%$ (2) and $R^2 = 0.96$ between the estimated Zsd from R_{rs} and the measured Zsd. More details about the method can be found in Lee et al. [12]

$$\varepsilon = \frac{1}{n} \cdot \sum_{i=1}^{n} \left[Z^i{}_{\mathrm{sd-est}} - Z^i{}_{\mathrm{sd-mea}} \right] / \left[Z^i{}_{\mathrm{sd-est}} + Z^i{}_{\mathrm{sd-mea}} \right] * 200\% \quad (2)$$

where i represents an individual data point, and n is the number of samples. $Z_{\mathrm{sd\text{-}mea}}$ and $Z_{\mathrm{sd\text{-}est}}$ are the measured and estimated values of Z_{sd}, respectively.

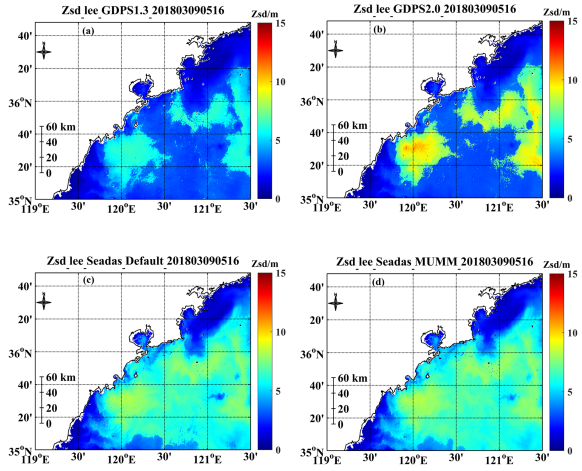

Fig. 4. Spatial distribution of transparency retrieved from GOCI data based on four different AC algorithms on 05:16, Mar 09, 2018 (UTC). (a) AC algorithm of GDPS1.3. (b) AC algorithm of GDPS2.0. (c) Standard AC algorithm of NASA. (d) AC algorithm of MUMM.

IV. Results

A. Adaptability Analysis of Zsd_lee 2015 Retrieval Algorithm

In this article, we apply the in-situ optics experimental data (blue stations in Fig. 1) obtained in Jiaozhou Bay and Qingdao offshore in Aug 2014 to estimate the transparency value using the theoretical model of Lee 2015. Then the estimated transparency values are compared with the in-situ measured values (see Fig. 2). The estimated transparency results based on the in-situ measurement data show that the transparency

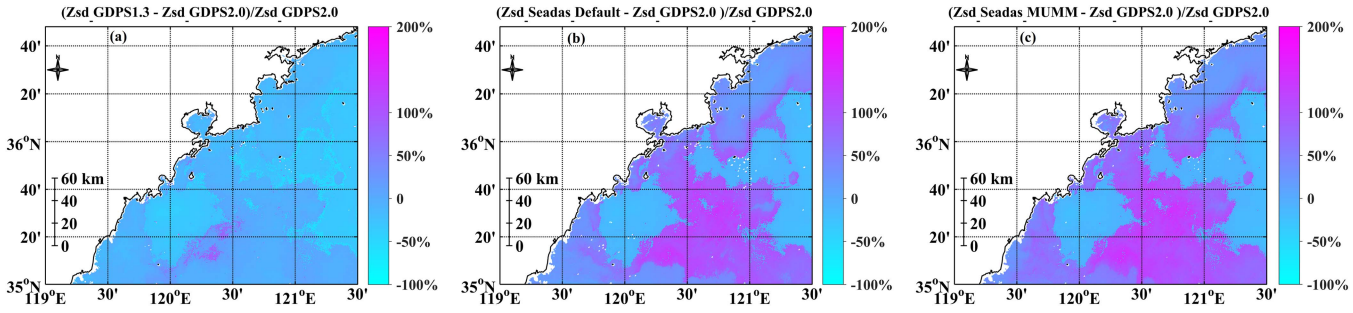

Fig. 5. Change ratio of transparency data relative to Zsd_GDPS2.0 based on (a) AC algorithm of GDPS1.3, (b) standard AC algorithm of NASA, and (c) AC algorithm of MUMM on 05:16, Mar 09, 2018 (UTC).

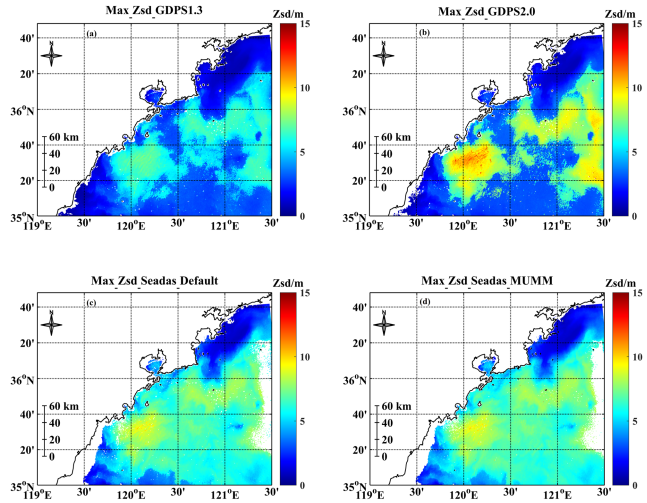

Fig. 6. Spatial distribution results of the maximum transparency values retrieved from eight GOCI data based on the four different AC algorithms in Mar 09, 2018. (a) AC algorithm of GDPS1.3. (b) AC algorithm of GDPS2.0. (c) Standard AC algorithm of NASA. (d) AC algorithm of MUMM.

retrieval model of Zsd_lee_2015 is suitable for Jiaozhu Bay and Qingdao coastal waters. The coefficient of determination (R^2) reaches 0.83, the averaged unbiased percentage difference (ε) is 16.4%, the root-mean-square error (RMSE) is 0.087 m, and the mean absolute percentage error (MAPE) is 18.3%. Among them, MAPE is not easily affected by extreme values and uses percentage to measure the size of data deviation, which is easy to understand. Those corresponding validation indicators were determined:

$$\mathrm{RMSE} = \sqrt{\frac{1}{n} \cdot \sum_{\mathrm{i}=1}^{n} \left(Z^{i}{}_{\mathrm{sd-mea}} - Z^{i}{}_{\mathrm{sd-est}}\right)^2} \tag{3}$$

$$\mathrm{MAPE} = \frac{1}{n} \cdot \sum_{\mathrm{i}=1}^{n} \frac{\left|Z^{i}{}_{\mathrm{sd-mea}} - Z^{i}{}_{\mathrm{sd-est}}\right|}{Z^{i}{}_{\mathrm{sd-mea}}} \times 100\%. \tag{4}$$

B. Retrieval Accuracy of Transparency Under Four AC Algorithms

Although the result based on field experimental data suggests that the transparency retrieve algorithm of Lee 2015 has adaptability in this study area. And the existing literature also indicates that it has good potential to be applied to Landsat and MODIS satellite data [13], [14]. However, the satellite cross-comparison results of GOCI and MODIS show that the R_{rs} data obtained from GOCI based on different AC algorithms are inconsistent with R_{rs} data of MODIS, and there are great differences in some bands [61]. In this article, whether the Zsd_lee 2015 retrieve algorithm is suitable for GOCI data in the studied sea area is analyzed, and the influence on the retrieval accuracy of transparency caused by different AC algorithms is considered.

The four operational AC algorithms introduced in Section II-B were applied to process the GOCI data and the R_{rs} data were obtained respectively. Then four sets of one-to-one corresponding retrieved transparency data were calculated based on the Zsd_lee 2015 algorithm. The retrieved transparency data were compared and analyzed with the measured data, as illustrated in Fig. 3, following the temporal-space matching principle: temporal difference less than 3 h and spatial distance less than 300 m. The comparison results between the transparency data obtained based on AC algorithm of GDPS2.0 with the measured data [see Fig. 3(b)] are generally better than the other three models [see Fig. 3(a), (c), and (d)]. Its coefficient of determination is 0.74, the averaged unbiased percentage difference is 26%, the bias is -0.34 m, and MAPE is 25%. Transparency retrieved from R_{rs} based on AC algorithms of GDPS1.3 and GDPS2.0 [see Fig. 3(a) and (b)] are generally lower than the measured transparency data with bias of -0.53 m and -0.34 m, respectively. The retrieved transparency results based on the standard AC algorithm of NASA [see Fig. 3(c)] and MUMM [see Fig. 3(d)] are higher than the measured transparency data overall, with deviations of 1.01 m and 1.23 m, respectively. The results show that the difference in transparency value caused by different AC algorithms cannot be completely ignored.

C. Temporal and Spatial Differences of Transparency Under Four AC Algorithms

GOCI I provides 8 scenes of imaging data per day, and GOCI II can provide 10 scenes. Their high-frequency observations make it possible to analyze the hourly changes of marine geochemical information. However, the influence of different AC algorithms on the analysis of hourly changes of biochemical parameters has not been considered so far. In this study, we selected 8 observation satellite data of GOCI obtained on Mar

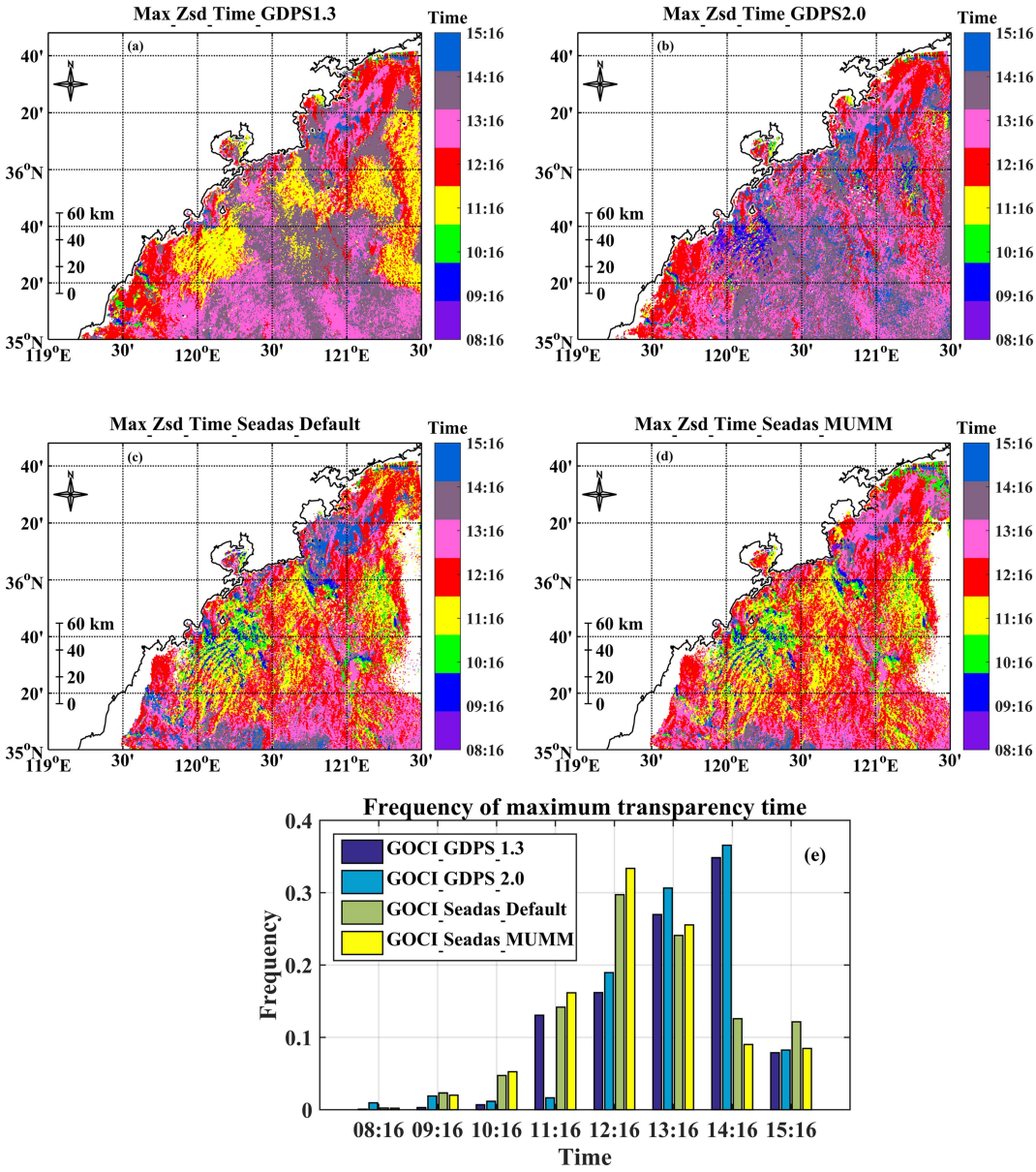

Fig. 7. Spatial distribution figures of the imaging time with the maximum transparency value in 8 h (08:16–15:16 local time) corresponding to each longitude and latitude pixel point based on (a)–(d) different AC algorithms, and (e) the frequency statistics of imaging time with maximum transparency value in Mar 09, 2018.

09, 2018, to conduct a preliminary discussion on the spatial distribution difference and hourly variation of transparency caused by different AC algorithms. The 8 GOCI image data of Mar 09, 2018, were selected in this article because there was basically no data loss caused by cloud coverage, which were convenient for the application of those data for analysis.

Fig. 4 shows the spatial distribution of transparency retrieved from GOCI satellite data on 05:16, Mar 09, 2018 (UTC) based on four AC algorithms. It can be seen that there are great differences in the spatial distribution. The sea areas with the maximum transparency value are basically the same, but there is a large difference in the transparency value [see Fig. 4(a)–(d)]. Then the transparency value retrieved based on GDPS2.0 was selected as the benchmark, denoted as Zsd_GDPS2.0. The change ratio of transparency data obtained based on other three AC algorithms (denoted as Zsd_GDPS1.3, Zsd_Seadas_default and Zsd_Seadas_MUMM) relative to Zsd_GDPS2.0 were calculated (5), and the spatial distribution results as shown in Fig. 5. Through comprehensive analysis of Figs. 4 and 5, it is found that the change ratios of Zsd_GDPS1.3, Zsd_Seadas_default and Zsd_Seadas_MUMM relative to Zsd_GDPS2.0 are less than 0 (see Fig. 5) in the area where Zsd_GDPS2.0 has a high value greater than 5m [see Fig. 4(b)]. In the sea areas where Zsd_GDPS2.0 is less than 5 m, the change ratios of Zsd_Seadas_default and Zsd_Seadas_MUMM relative to Zsd_GDPS2.0 is greater than 0 [see Fig. 5(b) and (c)], and the ratio tends to 100% in most sea areas, even with 200% in some areas

$$\text{Ratio} = (Z_{sd}\_\text{AC} - Z_{sd}\_\text{GDPS2.0})/Z_{sd}\_\text{GDPS2.0}. \quad (5)$$

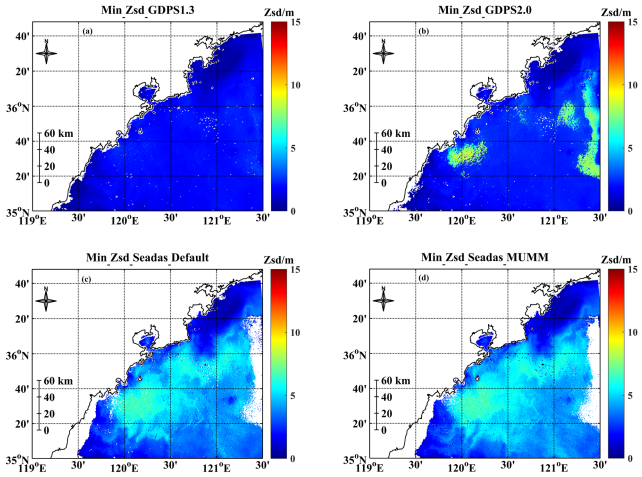

Fig. 8. Spatial distribution results of the minimum transparency values retrieved from eight GOCI data based on the four different AC algorithms in Mar 09, 2018. (a) AC algorithm of GDPS1.3. (b) AC algorithm of GDPS2.0. (c) Standard AC algorithm of NASA. (d) AC algorithm of MUMM.

By applying the 8-scene hourly imaging GOCI data of 2018.03.09 00:16-07:16 (UTC) (08:16-15:16 local time), the spatial distribution figures of the maximum transparency in 8 h corresponding to each longitude and latitude pixel point based on different AC algorithms are obtained (see Fig. 6). The imaging time with the maximum transparency were also visually displayed in the space layer [see Fig. 7(a)–(d)] and the imaging time with the maximum transparency was probability statistics [see Fig. 7(e)]. It is found that the spatial distribution results of maximum transparency during 08:16 to 15:16 (local time) based on different AC algorithms show great differences. The spatial distribution regions with maximum transparency less than 5 m based on GDPS1.3 and GDPS2.0 AC algorithms are similar and have little difference in values, while those with maximum transparency greater than 5 m are similar but have large difference in values [see Fig. 6(a) and (b)]. The spatial distribution of maximum transparency based on NASA standard AC algorithm [see Fig. 6(c)] and MUMM AC algorithm are consistent [see Fig. 6(d)]. However, the coverage areas whose value are greater than 5 m is significantly higher than the results of GDPS1.3 [see Fig. 6(a)] and GDPS2.0 [see Fig. 6(b)]. Based on the distribution results of imaging time with the maximum transparency, it is found that the maximum transparency value of Jiaozhou Bay and Qingdao coastal area based on GDPS1.3 and GDPS2.0 AC algorithms are mostly presented at 13:16 and 14:16 [see Fig. 7(a) and (b)]. However, the moments when the transparency value retrieved based on the other two AC algorithms present the maximum value are mostly at 12:16 and 13:16 [see Fig. 7(c) and (d)]. The frequency of the maximum transparency value presented at 11:16 based on the AC algorithms of GDPS1.3, NASA, and MUMM are basically the same, which are much higher than the result based on the AC algorithm of GDPS2.0 [see Fig. 7(e)].

By applying the 8-scene hourly imaging GOCI data of 2018.03.09 00:16-07:16 (UTC) (08:16–15:16 local time), the spatial distribution of the minimum transparency in 8 h corresponding to each longitude and latitude pixel point based on different AC algorithms are obtained (see Fig. 8). The imaging time with the minimum transparency were also visually displayed in the space layer [see Fig. 9(a)–(d)] and the imaging time with the minimum transparency was probability statistics [see Fig. 9(e)]. It is found that the spatial distribution results of the minimum transparency values based on GDPS1.3 and GDPS2.0 AC algorithms were similar in Mar 09, 2018, and the values were not different in a large range [see Fig. 8(a) and (b)]. The spatial distribution results of minimum transparency values based on NASA standard AC algorithm [see Fig. 8(c)] and MUMM AC algorithm are consistent [see Fig. 8(d)], but the minimum values are significantly higher than the results of GDPS1.3 [see Fig. 8(a)] and GDPS2.0 [see Fig. 8(b)]. After analyzing the distribution of the time when the minimum transparency value appears, we found that the imaging time with the minimum transparency value based on the four AC algorithms in 8 h are mostly at 08:16 [see Fig. 9(a)–(d)], and the occurrence frequency accounts for more than 78%, followed by 15:16, and the probability of the minimum transparency value appearing at 12:16–14:16 is very low and negligible [see Fig. 9(e)]. It should be noted that the probability of the minimum transparency value appearing at 09:16–11:16 based on NASA standard AC algorithm are greater than that of the other three AC algorithms.

D. Changing Characteristics of Transparency Based on Four AC Algorithms

Based on the spatial distribution results of the transparency of Jiaozhou Bay and Qingdao coastal area under the four AC algorithms in the "Result" module [see Figs. 4 and 5], and comprehensive considering the geographical characteristics of the studied area, we selected three red areas (red areas in Fig. 10, one in the bay and two outside the bay) and two blue transections that at the middle of the studied area (blue lines in Fig. 10) as the study object to analyze the changes of transparency based on different AC algorithms.

After analyzing the changes of transparency retrieved from GOCI data based on the four different AC algorithms at the transection along latitude direction (119.60°E–121.50°E, 35.50°N) and the transection along longitude direction (35.00–36.50°N, 121°E) at the imaging UTC time 05:16, Mar 09, 2018 (see Fig. 11). We find that in the transection along latitude direction, the change trends of transparency obtained based on the AC algorithm of NASA and MUMM are almost completely consistent, but they differ significantly with the transparency changes based on the AC algorithms of GDPS1.3 and GDPS2.0. And we get the same comparison results in the transection along longitude direction. The transparency values obtained based on the AC algorithm of GDPS2.0 are significantly higher than those obtained based on the other three methods in the range of 119.8–120.4 °E and 121.2–121.4°E of the transection along latitude direction. In other ranges of the transection along the latitude direction, the change trends of transparency obtained based on the AC algorithm of GDPS1.3 and GDPS2.0 are basically the same. And the transparency values are smaller than the results of the other two methods, and the difference can be up to 4 m. The transparency values obtained based on the AC algorithm

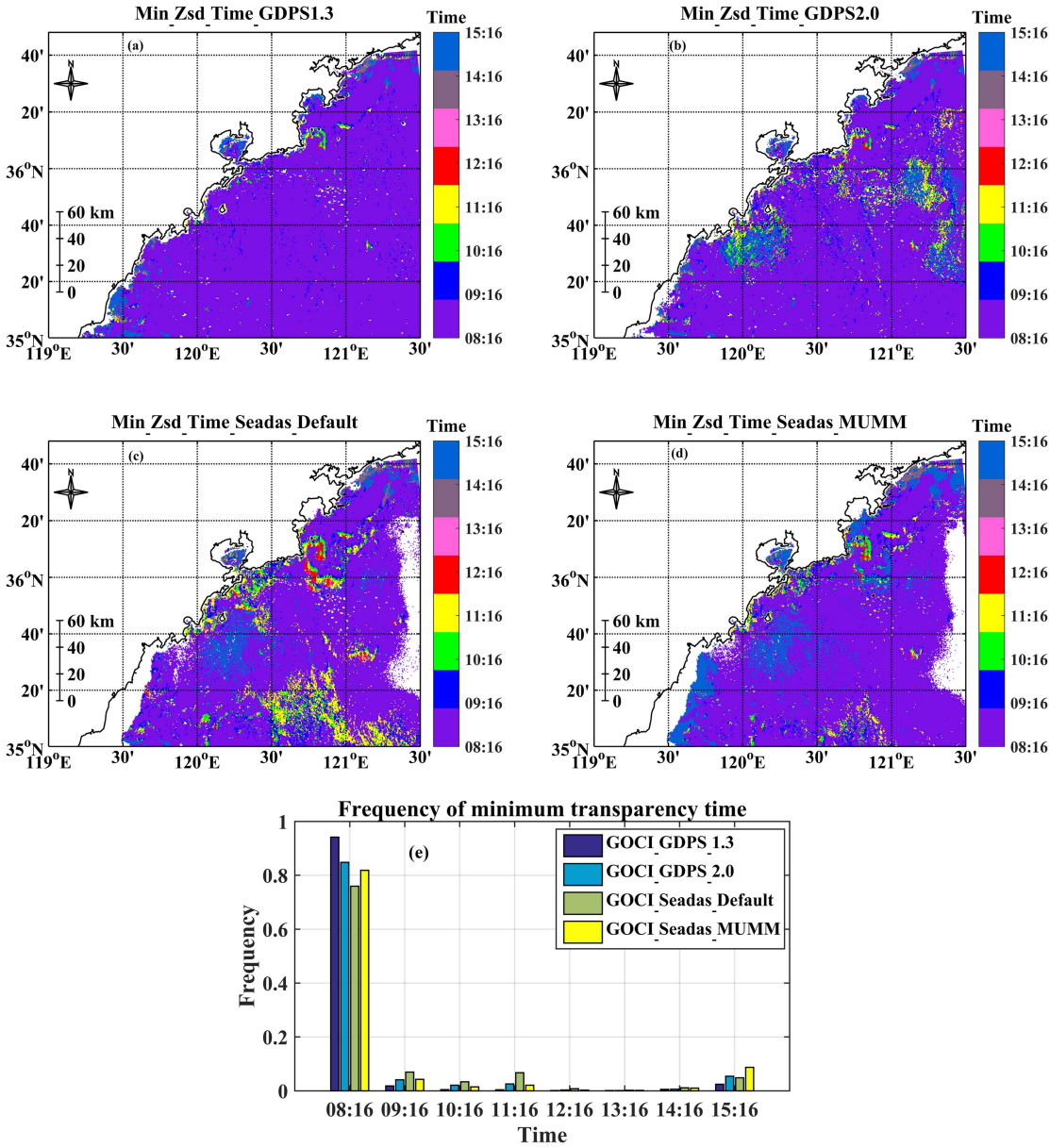

Fig. 9. Spatial distribution figures of the imaging time with the minimum transparency value in 8 h (08:16–15:16 local time) corresponding to each longitude and latitude pixel point based on (a)–(d) different AC algorithms, and (e) the frequency statistics of imaging time with minimum transparency value in Mar 09, 2018.

of GDPS2.0 are significantly higher than those obtained based on the other three methods in the range of 35.3–35.4°N and 35.75–35.9°N of the transection along longitude direction. In other ranges of the transection along longitude direction, the change trends of transparency obtained based on the AC algorithm of GDPS1.3 and GDPS2.0 are basically the same. And the transparency values are smaller than the results of the other two methods, and the difference can be up to 3 m.

Then the hourly changes of the average transparency values of the three regions selected in Fig. 10 within 8 h from 08:16 to 15:16 (local time) on Mar 09, 2018 were analyzed (see Fig. 12). In region I, the change trends of transparency values obtained based on the AC algorithms of GDPS2.0, NASA, and MUMM algorithm are basically same, showing the upward trend from 08:16 to 12:16, the downward trend from 12:16 to 15:16, and the maximum value appears at imaging time 12:16. However, the change trend of the transparency values obtained based on GDPS2.0 is different from the analysis results of the other three algorithms after 11:16, it shows a slight decline first, then an increase and then a decline. In region I, the occurrence moments of minimum and maximum transparency values based on different AC algorithms are not completely consistent. In region II, the change trends of transparency obtained based on the AC algorithm of NASA and MUMM are consistent, with an upward trend from 08:16 to 12:16, a downward trend from 12:16 to 15:16, and the maximum value appears at 12:16 imaging time. The transparency obtained based on GDPS2.0 showed a low value at 11:16 with a downward trend from 09:16 to 11:16, then an upward trend to 14:16, and the maximum value appeared at 14:16. However, the transparency values obtained

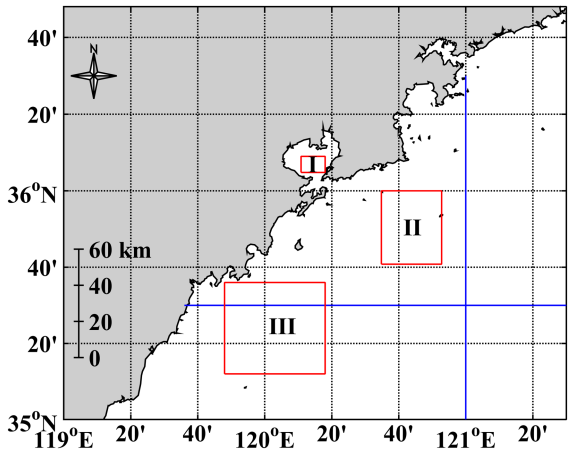

Fig. 10. Selected two transections (blue lines:119.60°E–121.50°E, 35.50°N; 35.00–36.50°N, 121°E) and three areas (red areas) in this article.

based on GDPS1.3 have a high value at 11:16, which is almost the same as the maximum value at 14:16. In region II, the lowest transparency value all appears at 08:16. In region III, the change trend of the transparency value obtained based on the AC algorithms of NASA and MUMM are consistent, which increases from 08:16 to 12:16, and decreases from 12:16 to 15:16, and the maximum value appears at the imaging time 12:16. The transparency values obtained based on GDPS1.3 show an increasing trend from 08:16 to 13:16, and the maximum value appears at 13:16. The maximum value of transparency based on GDPS2.0 appears at 14:16. In region III, the lowest value of transparency occurs at 08:16, but the highest value of transparency does not appear at the same moment. It can be seen that the conclusions based on different AC algorithms to study the hourly change of transparency in different areas will not be completely consistent.

V. Discussion

A. Uncertainties of Zsd Retrieval

The Zsd_lee_2015 model shows that Zsd is determined by the minimum value of the K_d spectrum in the visible range, which has a good correlation with ocean color [12]. Due to the particularity of the semi-closed Jiaozhou bay and Qingdao coastal area, the appropriate AC model and the applicability of algorithm are the problems that must be faced when using satellite remote sensing to monitor the changes of transparency in coastal waters. Currently, numerous AC algorithms have been published and utilized worldwide. However, there is a lack of comparison among satellite retrieval transparency data under different AC algorithms. The high-frequency observation characteristics of GOCI's 8 daily images provide us with convenient conditions to study the differences of retrieved transparency obtained based on various AC algorithms within a short time frame. Some researchers use GOCI data to analyze the temporal and spatial variation of transparency and its influencing factors in specific sea areas [50], [62]. For example, Zhou et al. used GOCI data to analyze the hourly variation of transparency in Jiaozhou Bay, and analyzed the relationship between transparency with tide and solar zenial angle based on Zsd_lee_2015 [62]. However, the results of the third section of this article may cast doubt on the validity of these published studies, because the hourly variation results of regional transparency values based on different AC algorithms are not completely consistent.

Although the agreement between the Zsd_Lee_2015 model and the measured data is very good in many ocean areas, even very suitable for some satellites [13], [14], [63]. However, the results of this article show that we cannot ignore the retrieval error caused by the AC algorithm when applying Zsd_lee_2015 model to retrieve transparency based on GOCI data. The AC algorithm and retrieval model should be considered simultaneously during the whole retrieval process. This poses a challenge to how to select the appropriate AC algorithm in the process of Zsd retrieval in offshore waters. Perhaps we need to develop new evaluation systems to evaluate the suitability of AC algorithms.

B. Potential Link Between Aerosol Optical Thickness and Retrieved Transparency Data

The role of AC is to remove atmospheric effects on remote sensing data, the most important of which is the effect of aerosols [61]. The distribution of aerosols is not uniform because of the great influence of human activities in the coastal waters. The R_{rs} products of coastal waters are very vulnerable to the influence of complex multiple scattering in the atmosphere-land system, and the accuracy of the AC is highly dependent on the accurate understanding of the surface types and aerosol patterns in the study area [64]. To clarify the potential relationship between aerosol optical thickness and retrieval transparency, the aerosol optical thickness data at the MODIS/Aqua 555 nm at 05:25 on Mar 9, 2018 (see Fig. 13) was used to analyze the influence of aerosols on the transparency results of GOCI under different AC algorithms. The MODIS aerosol data used in this article was only 9 min different from the GOCI data imaging time. The transparency data obtained at 05:16 on Mar 9, 2018, from GOCI based on the GDPS 2.0 and NASA standard AC algorithms were selected and analyzed in conjunction with the aerosol optical thickness data. The results are shown in Fig. 14. In the range of aot_555<0.055 and aot_555>0.12, the transparency data obtained based on the NASA standard AC algorithm are higher than those obtained based on the GDPS 2.0. Within the range of aot_555 values from 0.055 to 0.12, the difference between the transparency values obtained by the two AC algorithms is between 0 and 4 m. This indicates that aerosol models need to be further optimized and regionalized in the process of AC of satellite data in coastal waters. Those results may provide new ideas for optimizing AC algorithm models for GOCI. The customization of aerosol type should be further considered, for instance.

It is worth noting that the analysis results obtained are not limited to the data presented in the article. Similar conclusions are obtained when we use other GOCI data. Although the results of this study show that there are differences in hourly changes of transparency retrieved from GOCI data under different AC algorithms, due to the lack of measured hourly transparency values that match the GOCI satellite data, there is no better method

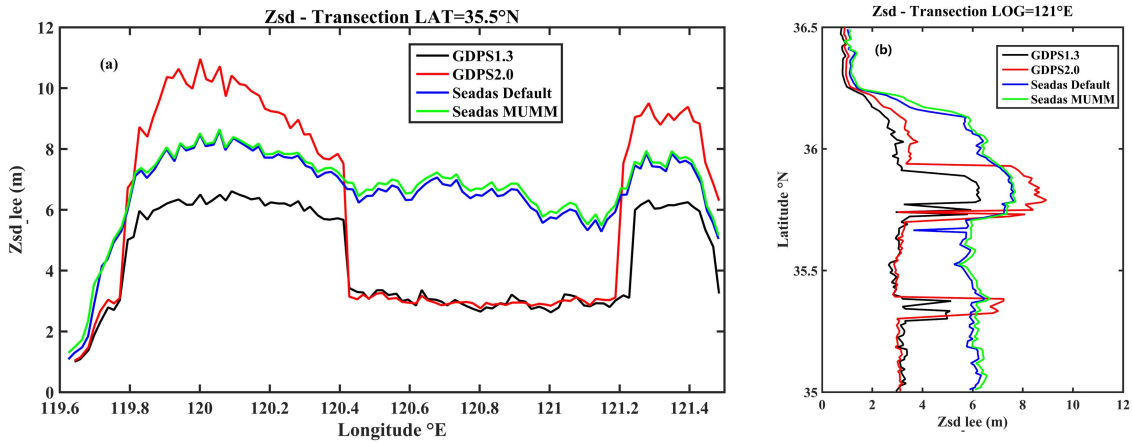

Fig. 11. Changing curves of transparency retrieved from GOCI data based on the four different AC algorithms (a) at the transection along latitude direction and (b) the transection along longitude direction at the imaging time 05:16, Mar 09, 2018 (UTC).

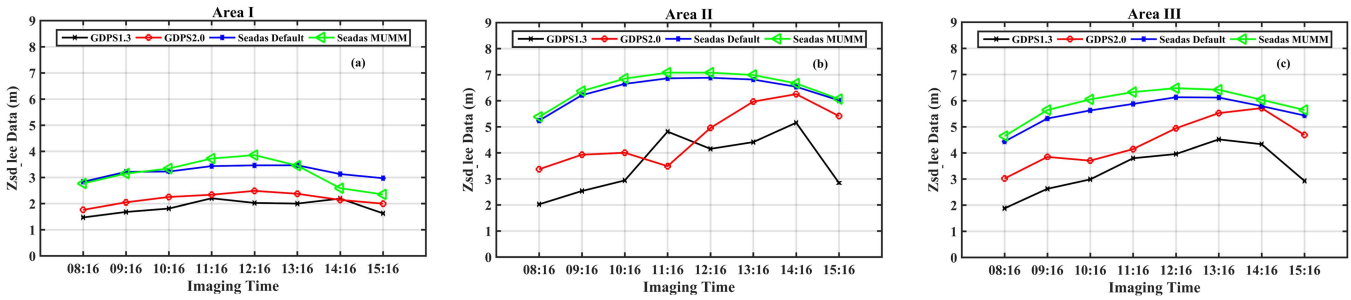

Fig. 12. Comparison curves of hourly changes of transparency retrieved from GOCI data based on the four different AC algorithms in (a) region I, (b) region II, (c) and region III.

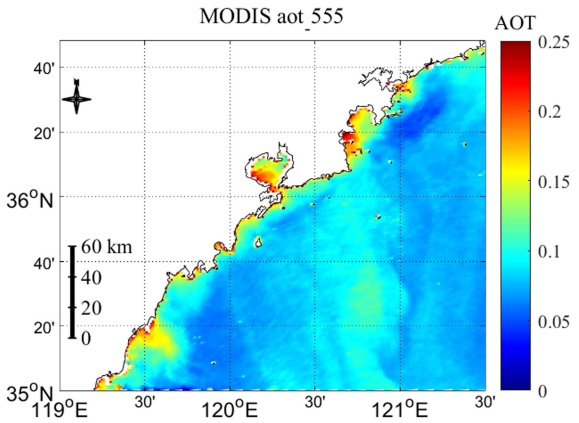

Fig. 13. AOT data in 555 nm of MODIS/Aqua at the imaging time 05:25, Mar 09, 2018 (UTC).

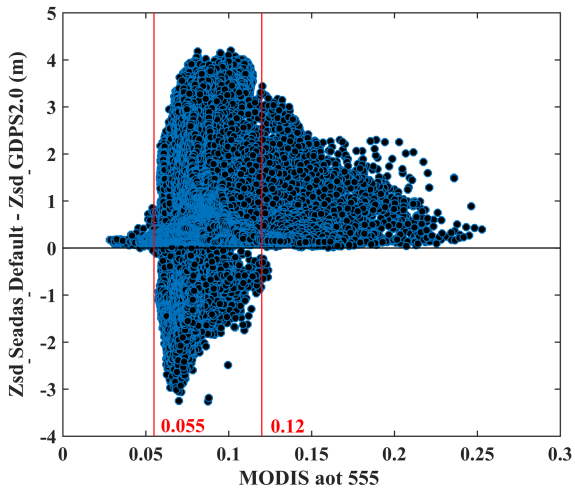

Fig. 14. Scatter plots of aerosol optical thickness (Modis aot_555) versus transparency difference (Zsd_Seadas_Default - Zsd_GDPS2.0).

to quantitatively analyze the hourly changes obtained by GOCI based on the four AC algorithms. The other things that require in-depth analysis in the future are what is the mechanism behind these differences, which link of different AC methods caused the difference, and which AC is more reasonable under what conditions. One of the purposes of this article is to encourage research groups to supplement the quantitative analysis of the hourly change results.

VI. Conclusion

Water transparency is an essential indicator of water quality. In this article, we evaluated the suitability of water transparency retrieval model proposed by Lee in 2015 using in situ data. The impacts of four AC algorithms on the retrieval of water transparency were also assessed. And the hourly changes of

transparency in Jiaozhou Bay and Qingdao coastal area based on four AC algorithms were compared for the first time. The results showed that Lee's water transparency was suitable in the study area (R^2>0.8, MAPE = 16.4%) and the AC model has non-negligible impacts on the water transparency retrieval from GOCI. Under different AC algorithms, the difference of transparency values retrieved from GOCI by using the same retrieval model in the same study area can be as high as double. It is also found that the timely changing characters of transparency obtained by different AC models are not completely consistent, and even the maximum and minimum values of transparency and the time of maximum and minimum values appeared in the 8 h are not the same. For example, on Mar 09, 2018, the maximum transparency value of Jiaozhou Bay and Qingdao coastal area based on GDPS1.3 and GDPS2.0 AC algorithms are mostly presented at 13:16 and 14:16, while the moments when the transparency value retrieved based on the other two AC algorithms present the maximum value are mostly at 12:16 and 13:16. The results of this article show that different AC models have a huge impact on the accuracy of retrieved ocean color products, it is urgent to develop a new evaluation system for evaluating the performance of AC models.

ACKNOWLEDGMENT

The authors would like to thank the KOSC for providing GOCI data and various versions of GDPS software. And the authors are also grateful to NASA Ocean Biology Processing Group for providing MODIS/Aqua data and SeaDAS software.

REFERENCES

[1] L. K. Chawla and A. K. Mishra, "A review of remote sensing applications for water security: Quantity, quality, and extremes," *J. Hydrol.*, vol. 585, 2020, Art. no. 124826.

[2] Z. qin, " On distribution characteristics of water transparency in the east China sea," *Mar. Sci. Bull.*, vol. 2, no. 6, pp. 21–24, 1983.

[3] L. zhi, "The application of water color and transparency in Marine environmental science," *Mar. Environ. Sci.*, vol. 1, no. 2, pp. 93–98, 1982.

[4] Z. qin, "Seawater transparency," *Trans. Oceanol. Limnol.*, vol. 4, pp. 14–18, 1982.

[5] E. D. R. Maúre, G. Terauchi, J. Ishizaka, N. Clinton, and M. DeWitt, "Globally consistent assessment of coastal eutrophication," *Nature Commun.*, vol. 12, no. 1, 2021, Art. no. 6142.

[6] F. le, "Study on the water colour and transparency in the Bohai sea," *Adv. Mar. Sci.*, vol. 4, no. 1, pp. 33–40, 1986.

[7] Z. R. Zhulan bu, "Distributions and variations of the transparency in the Bohai sea, Yellow sea and East China sea," *Trans. Oceanol. Limnol.*, vol. 3, pp. 1–11, 1991.

[8] P. l. Hexian qiang and H. hui, "Monitor of water transparency in the China Sea by using satellite remote sensing," *Eng. Sci.*, vol. 6, no. 9, pp. 33–37, 2004.

[9] K. S. P., "Ocean color algorithms for estimating water clarity (Secchi depth) from Sea WiFS," *J. Adv. Mar. Sci. Technol. Soc.*, vol. 4, pp. 301–306, 1998.

[10] S. K., "Assessing secchi and photic zone depth in the Baltic Sea from satellite data," *Ambio*, vol. 32, pp. 577–585, 2003.

[11] M. B. Doron M, A Mangin, and O. Hembise, "Estimation of light penetration, and horizontal and vertical visibility in oceanic and coastal waters from surface reflectance," *J. Geophys. Res.*, vol. 112, pp. 1–15, 2007.

[12] Z. Lee et al., " Secchi disk depth: A new theory and mechanistic model for underwater visibility," *Remote Sens. Environ.*, vol. 169, pp. 139–149, 2015.

[13] Z. Lee, S. Shang, L. Qi, J. Yan, and G. Lin, "A semi-analytical scheme to estimate Secchidisk depth from Landsat-8 measurements," *Remote Sens. Environ*, vol. 177, pp. 101–106, 2016.

[14] S. Shang, Z. Lee, L. Shi, G. Lin, G. Wei, and X. Li, "Changes in water clarity of the Bohai Sea: Observations from MODIS," *Remote Sens. Environ.*, vol. 186, pp. 22–31, 2016.

[15] Z. Lee, S. Shang, K. Du, and J. Wei, "Resolving the long-standing puzzles about the observed Secchi depth relationships," *Limnol. Oceanogr.*, vol. 63, no. 6, pp. 2321–2336, 2018.

[16] D. Jiang, B. Matsushita, F. Setiawan, and A. Vundo, "An improved algorithm for estimating the Secchi disk depth from remote sensing data based on the new underwater visibility theory," *ISPRS J. Photogrammetry Remote Sens.*, vol. 152, pp. 13–23, 2019.

[17] K. Kabiri, "Estimation of the Secchi disk depth from the NASA MODIS-Aqua diffuse attenuation coefficient data in the northern Persian Gulf and the Gulf of Oman: A spatiotemporal assessment," *Regional Stud. Mar. Sci.*, vol. 52, 2022, Art. no. 102359.

[18] A. C. Gomes, E. Alcântara, T. Rodrigues, and N. Bernardo, "Satellite estimates of euphotic zone and secchi disk depths in a colored dissolved organic matter-dominated inland water," *Ecological Indicators*, vol. 110, 2020, Art. no. 105848.

[19] D. Liu et al., "Observations of water transparency in China's lakes from space," *Int. J. Appl. Earth Observ. Geoinf.*, vol. 92, 2020, Art. no. 102187.

[20] S. Wang et al., "Changes of water clarity in large lakes and reservoirs across China observed from long-term MODIS," *Remote Sens. Environ.*, vol. 247, 2020, Art. no. 111949.

[21] M. Al Kaabi, J. Zhao, and H. Ghedira, "MODIS-based mapping of secchi disk depth using a qualitative algorithm in the shallow Arabian Gulf," *Remote Sens.*, vol. 8, no. 5, 2016, Art. no. 423.

[22] L. Feng, X. Hou, and Y. Zheng, "Monitoring and understanding the water transparency changes of fifty large lakes on the Yangtze Plain based on long-term MODIS observations," *Remote Sens. Environ.*, vol. 221, pp. 675–686, 2019.

[23] X. He et al., "Recent changes of global ocean transparency observed by SeaWiFS," *Continental Shelf Res.*, vol. 143, pp. 159–166, 2017.

[24] K. Shi, Y. Zhang, G. Zhu, B. Qin, and D. Pan, "Deteriorating water clarity in shallow waters: Evidence from long term MODIS and in-situ observations," *Int. J. Appl. Earth Observ. Geoinf.*, vol. 68, pp. 287–297, 2018.

[25] S. Zeng et al., "Retrieval of secchi disk depth in turbid lakes from GOCI based on a new semi-analytical algorithm," *Remote Sens.*, vol. 12, no. 9, 2020, Art. no. 1516.

[26] T. Jia, Y. Zhang, C. Weng, and R. Dong, "Improving remote sensing retrieval of global ocean transparency with optical water classification," *Ecological Indicators*, vol. 143, 2022, Art. no. 109359.

[27] D. Yu, L. Yang, Y. Li, J. Xiang, and C. Zhao, "Spatiotemporal changes and influencing factors of water clarity in the Yellow Sea over the past 20 years," *Mar. Pollut. Bull.*, vol. 191, 2023, Art. no. 114904.

[28] J. Guo, H. Pan, R. Cao, J. Wang, and X. Lv, "Multiple timescale variations in water transparency in the Eastern China Seas over the period 1997–2019," *J. Geophys. Res., Oceans*, vol. 128, no. 4, 2023, Art. no. e2022JC019170.

[29] Z. Lee, K. L. Carder, and R. A. Arnone, "Deriving inherent optical properties from water color: A multi-band quasi-analytical algorithm for optically deep waters," *Appl. Opt.*, vol. 41, no. 27, pp. 5755–5772, 2002.

[30] H. R. Gordon, "Removal of atmospheric effects from satellite imagery of the oceans," *Appl. Opt.*, vol. 17, no. 10, pp. 1631–1636, 1978.

[31] K. G. Ruddick, F. Ovidio, and M. Rijkeboer, "Atmospheric correction of SeaWiFS imagery for turbid coastal and inland waters," *Appl. Opt.*, vol. 39, no. 6, pp. 897–912, 2000.

[32] D. Antoine and A. Morel, "A multiple scattering algorithm for atmospheric correction of remotely sensed ocean color (MERIS instrument): Principle and implementation for atmospheres carrying various aerosols including absorbing ones," *Int. J. Remote Sens.*, vol. 20, no. 9, pp. 1875–1916, 1999.

[33] C. Goyens, C. Jamet, and T. Schroeder, "Evaluation of four atmospheric correction algorithms for MODIS-aqua images over contrasted coastal waters," *Remote Sens. Environ.*, vol. 131, pp. 63–75, 2013.

[34] M. Wang and W. Shi, "The NIR-SWIR combined atmospheric correction approach for MODIS ocean color data processing," *Opt. Exp.*, vol. 15, pp. 15722–15733, 2007.

[35] M. Wang and W. Shi, "Remote sensing of the ocean contributions from ultraviolet to near-infrared using the Shortwave Infrared bands: Simulations," *Appl. Opt.*, vol. 46, no. 9, pp. 1535–1547, 2007.

[36] M. Oo, M. Vargas, A. Gilerson, B. Gross, F. Moshary, and S. Ahmed, "Improving atmospheric correction for highly productive coastal waters using the short wave infrared retrieval algorithm with water-leaving reflectance constraints at 412 nm," *Appl. Opt.*, vol. 47, pp. 3846–3859, 2008.

[37] X. He, Y. Bai, D. Pan, J. Tang, and D. Wang, "Atmospheric correction of satellite ocean color imagery using the ultraviolet wavelength for highly turbid waters," *Opt. Exp.*, vol. 20, no. 18, pp. 20754–20770, 2012.
[38] C. Hu, K. L. Carder, and F. E. Muller-Karger, "Atmospheric correction of SeaWiFS imagery over turbid coastal waters: A practical method," *Remote Sens. Environ.*, vol. 74, pp. 195–206, 2000.
[39] M. Wang, W. Shi, and L. Jiang, "Atmospheric correction using near-infrared bands for satellite ocean color data processing in the turbid western Pacific region," *Opt. Exp.*, vol. 20, pp. 741–753, 2012.
[40] J.-H. Ahn and Y.-J. Park, "Estimating water reflectance at near-infrared wavelengths for turbid water atmospheric correction: A preliminary study for GOCI-II," *Remote Sens.*, vol. 12, pp. 3791–3803, 2020.
[41] J.-H. Ahn, Y.-J. Park, and H. Fukushima, "Comparison of aerosol reflectance correction schemes using two near-infrared wavelengths for ocean color data processing," *Remote Sens.*, vol. 10, pp. 1791–1803, 2018.
[42] J.-H. AHN, Y.-J. PARK, W. KIM, and B. LEE, "Simple aerosol correction technique based on the spectral relationships of the aerosol multiple-scattering reflectances for atmospheric correction over the oceans," *Opt. Exp.*, vol. 24, no. 26, pp. 29659–29669, Dec. 2016.
[43] C. Jamet, S. Thiria, and C. Moulin, "Use of a neurovariational inversion for retrieving oceanic and atmospheric constituents from Ocean color imagery: A feasibility study," *J. Atmos. Ocean. Technol.*, vol. 22, pp. 460–475, 2005.
[44] T. Schroeder, I. Behnert, M. Schaale, J. Fischer, and R. Doerffer, "Atmospheric correction algorithm for MERIS above case-2 waters," *J. Remote Sens.*, vol. 28, pp. 1469–1486, 2007.
[45] J. Brajard, R. Santer, M. Crpon, and S. Thiria, "Atmospheric correction of MERIS data for case-2 waters using a neuro-variational inversion," *Remote Sens. Environ.*, vol. 126, pp. 51–61, 2012.
[46] J. Brajard, C. Jamet, S. Thiria, C. Moulin, and M. Crepon, "Use of a neuro-variational inversion for retrieving oceanic and atmospheric constituents from satellite ocean color sensor: Application to absorbing aerosols," *Neural Netw.*, vol. 22, pp. 460–475, 2006.
[47] C. P. Kuchinke, H. R. Gordon, L. W. Harding, and K. J. Voss, "Spectral optimization for constituent retrieval in Case II waters II: Validation study in the Chesapeake Bay," *Remote Sens. Environ.*, vol. 113, pp. 610–621, 2009.
[48] R. Chomko, H. Gordon, S. Maritorena, and D. Siegel, "Simultaneous retrieval of oceanic and atmospheric parameters for ocean color imagery by spectral optimization: A validation," *Remote Sens. Environ.*, vol. 84, no. 2, pp. 208–220, 2003.
[49] S. A. Garver and D. A. Siegel, "Inherent optical property inversion of ocean color spectra anditsbiogeochemical interpretation: 1. Time series from the Sargasso Sea," *J. Geophys. Res.*, vol. 102, no. C8, pp. 18607–18625, 1997.
[50] X. Ding et al., "Using geostationary satellite ocean color data and super-pixel to map the diurnal dynamics of water transparency in the eastern China seas," *Ecological Indicators*, vol. 142, 2022, Art. no. 109219.
[51] P. Li et al., "Human impact on suspended particulate matter in the Yellow River Estuary, China: Evidence from remote sensing data fusion using an improved spatiotemporal fusion method," *Sci. Total Environ.*, vol. 750, Jan. 2021, Art. no. 141612.
[52] J. Liu et al., "Diurnal dynamics and seasonal variations of total suspended particulate matter in highly turbid Hangzhou Bay waters based on the geostationary ocean color imager," *IEEE J. Sel. Topics Appl. Earth Observ. Remote Sens.*, vol. 11, no. 7, pp. 2170–2180, Jul. 2018.
[53] J.-H. Ryu, H.-J. Han, S. Cho, Y.-J. Park, and Y.-H. Ahn, "Overview of geostationary ocean color imager (GOCI) and GOCI data processing system (GDPS)," *Ocean. Sci. J.*, vol. 47, no. 3, pp. 223–233, 2012.
[54] J.-H. Ahn, Y.-J. Park, J.-H. Ryu, B. Lee, and I. S. Oh, "Development of atmospheric correction algorithm for Geostationary Ocean Color Imager(GOCI)," *Ocean. Sci. J.*, vol. 47, no. 3, pp. 247–259, 2012.
[55] J. H. Ahn, Y. J. Park, W. Kim, and B. Lee, "Vicarious calibration of the geostationary ocean color imager," *Opt. Exp.*, vol. 23, no. 18, pp. 23236–23258, 2015.
[56] H. R. Gordon and M. Wang, "Retrieval of water leaving radiance and aerosol optical thickness over the oceans with SeaWiFS: A preliminary algorithm," *Appl. Opt.*, vol. 33, no. 3, pp. 443–452, 1994.
[57] R. P. Stumpf, R. A. Arnone, R. W. Gould, P. M. Martinolich, and V. Ransibrahmanakul, "A partially coupled ocean-atmosphere model for retrieval of water-leaving radiance from SeaWiFS in coastal waters," *NASA Tech. Memorandum*, vol. 206892, pp. 51–59, 2003.
[58] S. W. Bailey, B. A. Franz, and P. J. Werdell, "Estimation of near-infraredwater-leaving reflectance for satellite ocean color data processing," *Opt. Exp.*, vol. 18, no. 7, pp. 7521–7527, 2010.
[59] Z. Ahmad et al., "New aerosol models for the retrieval of aerosol optical thickness and normalized water-leaving radiances from the SeaWiFS and MODIS sensors over coastal regions and open oceans," *Appl. Opt.*, vol. 49, pp. 5545–5560, 2010.
[60] Z. Lee, B. Lubac, J. Werdell, and R. Arnone, "Update of the quasi-analytical algorithm (QAA_v6)," [Online]. Available: https://ioccg.org/groups/Software_OCA/QAA_v6_2014209.pdf
[61] X. Liu, Q. Yang, Y. Wang, and Y. Zhang, "Evaluation of GOCI remote sensing reflectance spectral quality based on a quality assurance score system in the Bohai Sea," *Remote Sens.*, vol. 14, no. 5, 2022, Art. no. 1075.
[62] Y. Zhou et al., "Monitoring multi-temporal and spatial variations of water transparency in the Jiaozhou Bay using GOCI data," *Mar. Pollut. Bull.*, vol. 180, Jul. 2022, Art. no. 113815.
[63] Y. Mao, S. Wang, Z. Qiu, D. Sun, and M. Bilal, "Variations of transparency derived from GOCI in the Bohai Sea and the Yellow Sea," *Opt. Exp.*, vol. 26, no. 9, pp. 12191–12209, 2018.
[64] Q. Vanhellemont and K. Ruddick, "Atmospheric correction of metre-scale optical satellite data for inland and coastal water applications," *Remote Sens. Environ.*, vol. 216, pp. 586–597, 2018.

Xiao-Yan Liu received the M.S. degree in marine information detection and processing, in 2014, from Ocean University of China, Qingdao, China, where she is currently working toward the Ph.D. degree in resources and environment.

She has been an Engineer with the Institute of Oceanographic Instrumentation, Qilu University of Technology (Shandong Academy of Sciences) since 2014. She has authored more than 20 articles and holds two patents. Her research interests include ocean remote sensing and ocean optics.

Jing-Wen Hu received the Ph.D. degree in marine information detection and processing from Ocean University of China, Qingdao, China, in 2016.

She is currently an Associate Researcher with Shandong Marine Forecast and Hazard Mitigation Service. Her research interests include ocean remote sensing and marine disaster prevention.

Lin Tian received the M.S. degree in photogrammetry and remote sensing from the Ocean University of China, in 2013, and the Ph.D. degree in atmospheric remote sensing and atmospheric sounding from Nanjing University of Information Science and Technology, Nanjing, China, in 2021.

He worked in the National Satellite Meteorological Center (NSMC), China Meteorological Administration (CMA). He is currently working as a Senior Engineer in NSMC/CMA. His research interests include atmospheric and remote sensing.

Ding-Feng Yu received the Ph.D. degree in environmental science from Yantai Institute of Coastal Zone Research, Chinese Academy of Sciences, Yantai, China, in 2013.

He is currently an Associate Professor with Institute of Oceanographic Instrumentation, Qilu University of Technology (Shandong Academy of Sciences), Qingdao, China. His main research interests include ocean color remote sensing and signal processing.

Hao Gao received the M.S. degree in automation and control from Newcastle University, Newcastle, U.K., in 2013. He is currently working toward the Ph.D. degree in marine surveying and charting with First Institute of Oceanography, Ministry of Natural Resources, Qingdao, China.

His research interests include marine environmental monitoring, Big Data analysis, remote sensing, digital image processing, and deep learning techniques.

Lei Yang received the B.S. and M.S. degrees in communication engineering from Harbin Institute of Technology, Harbin, China, in 2011 and 2013, respectively.

He is currently a Research Scientist with Institute of Oceanographic Instrumentation, Qilu University of Technology (Shandong Academy of Sciences), Qingdao, China. His research interests include data analysis and processing, system design, remote sensing, and array signal processing.

De-Yu An received the Ph.D. degree in environmental science from Yantai Institute of Coastal Zone Research, Chinese Academy of Sciences, Yantai, China, in 2020.

She is a Research Assistant with Institute of Oceanographic Instrumentation, Qilu University of Technology (Shandong Academy of Sciences), Qingdao, China. She has authored or coauthored more than 10 journal papers. Her main research interests include marine environment remote sensing and ocean color remote sensing.